Acta Crystallographica Section B
Structural Science
ISSN 0108-7681

X-ray atomic orbital analysis of 4*f* and 5*d* electron configuration of SmB_6 at 100, 165, 230 and 298 K

Shiro Funahashi,[a] Kiyoaki Tanaka[a]* and Fumitoshi Iga[b]

[a]Graduate School of Materials Science and Engineering, Nagoya Institute of Technology, Japan, and [b]Department of Quantum Matter, ADSM, Hiroshima University, Japan

Correspondence e-mail: tanaka.kiyoaki@nitech.ac.jp

Received 29 November 2009
Accepted 11 March 2010

Accurate electron-density measurement of SmB_6 at 100, 165, 230 and 298 K, and X-ray atomic orbital (XAO) analysis were carried out. The 4*f*-electron density around Sm and 5*d* electron density at ~ 1 Å from Sm were analysed by XAO analysis. The 5*d* electron density is due to the electrons of the $5d_{J=5/2}\Gamma_8$ orbitals which stem from the e_g orbitals in the strong field approximation. The change in electron populations of the $5d_{5/2}\Gamma_8$ orbitals with temperature is similar to that of the resistivity. Since the conduction band consists of $5d_{5/2}\Gamma_8$ and B-2*p* orbitals according to band theory, this indicates that the larger populations of the $5d_{5/2}\Gamma_8$ orbitals correspond to the larger number of localized electrons and are correlated to the resistivity of SmB_6. The occupation of the bulky $5d_{5/2}\Gamma_8$ orbitals may be the reason for the elongation of the lattice parameter below 150 K. The $4f_{7/2}\Gamma_6$ orbitals are obviously occupied except at 100 K, which seems to be caused by the energy gap between $4f_{5/2}$ and $4f_{7/2}$ states, which begins to exist between 100 and 150 K, and may represent one of the properties of a Kondo insulator.

1. Introduction

The properties of substances are mainly attributed to the behaviour of valence electrons. Therefore, it is important to observe the electron-density distribution (EDD) and manifest the physical properties from it in developing new materials. SmB_6 behaves as a metal above room temperature and becomes more of a semi-conductor as the temperature is lowered. The resistivity of SmB_6 increases steeply below 30 K. Therefore, it is very interesting to measure the change in EDD with temperature and analyze the valence orbitals which play an important role in this change using XAO analysis.

Recently many rare-earth complexes with interesting properties have been reported and caught our attention. However, the observation and quantitative analyses of EDD have been regarded as very difficult since the ratio of the number of valence electrons to the total number of electrons in the unit cell is small, and a highly accurate measurement is necessary. Since the required accuracy of the measurement seems to be close to the limit of the present accuracy of X-ray intensity measurements, the EDD was measured at several temperatures. The physical significance of the temperature change of the EDD could then be compared with the reported properties of the compound to assess the results. Measurement using a four-circle diffractometer, avoiding multiple diffraction with the ψ-scan method, has made the measurement of 4*f*-EDD possible. 4*f*-EDD was first analyzed by Tanaka, Kato & Ōnuki (1997) based on the real 4*f* orbitals in CeB_6 at 165 K. By employing the complex 4*f* orbitals which are calculated based on the spin-orbit interaction, the 4*f*-EDD

Table 1
Experimental details.

For all structures: cubic, $Pm\bar{3}m$, $Z = 1$. Experiments were carried out with Mo $K\alpha$ radiation using a four-circle diffractometer. Absorption correction was for a sphere. The transmission coefficient for spheres tabulated in Table 5.3.6B of the *International Tables for X-ray Crystallography* (1972) was interpolated with Lagrange's method (four point interpolation). Refinement was with 0 restraints.

	100 K	165 K	230 K	298 K
Crystal data				
Chemical formula	$B_6^{3-}Sm^{3+}$	$B_6^{3-}Sm^{3+}$	$B_6^{3-}Sm^{3+}$	$B_6^{3-}Sm^{3+}$
M_r	215.23	215.23	215.23	215.23
a (Å)	4.1327 (2)	4.1325 (2)	4.1338 (2)	4.1346 (2)
V (Å^3)	70.58 (1)	70.57 (1)	70.64 (1)	70.68 (1)
μ (mm^{-1})	20.50	20.51	20.49	20.43
Crystal radius (mm)	0.039	0.039	0.039	0.039
Data collection				
T_{min}, T_{max}	0.356, 0.418	0.356, 0.418	0.356, 0.418	0.356, 0.418
No. of measured, independent and observed [$F > 3.0\sigma(F)$] reflections	598, 187, 182	593, 182, 182	664, 187, 187	2162, 191, 191
R_{int}	0.011	0.013	0.011	0.044
Scan speed in ω (min^{-1})	2	2	2	2
Maximum No. of scans	10	10	10	10
Refinement				
$R[F^2 > 2\sigma(F^2)]$, $wR(F^2)$, S	0.009, 0.010, 0.86	0.008, 0.012, 1.11	0.010, 0.140, 1.04	0.008, 0.011, 0.98
No. of reflections	593	582	648	2149
No. of parameters	35	36	33	35
$\Delta\rho_{max}$, $\Delta\rho_{min}$ (e Å^{-3})	0.61, −0.29	0.39, −0.41	0.68, −0.70	0.41, −0.25

Computer programs: *MXC* (MAC Science), *IUANGLE* (Tanaka *et al.*, 1994), RSLC-3 UNICS system (Sakurai & Kobayashi, 1979), *RDEDIT* (Tanaka, 2008), *QNTAO* (Tanaka *et al.*, 2008).

of CeB_6 was analysed at 100, 165, 230 and 298 K (Tanaka & Ōnuki, 2002). In our previous work on CeB_6 (Makita *et al.*, 2007, 2008) 5*d* orbitals were also occupied above room temperature.

In the present study the EDD of isomorphic SmB_6, which formally has five 4*f* electrons and is a more complicated system than CeB_6, was measured and analyzed. This is our first XAO analysis of a system with multiple 4*f* electrons. The rare-earth ions are usually treated with the Russell–Saunders coupling (*L*–*S* coupling). However, evaluation of the matrix elements of the crystal fields added as a perturbation to the Hamiltonian is not straightforward, since the expression of all states in terms of the products of basic states is not derived because of too many states to be considered. When the operator-equivalent method of Stevens (1952) is used, the expression of the relevant states or basis functions for the multi-4*f*-electron system in terms of the products of the basic states can be skipped and the matrix elements of a secular equation of the final states with actual *J* values between $|L - S|$ and $L + S$ are calculated, where *L* and *S* are the total electronic orbital and spin-angular momenta. Using this method Walter (1986) formulated the electron density of trivalent rare-earth ions in the cubic crystal field assuming Hund's-rule ground states as the final states. The electron density is Fourier transformed to X-ray scattering factors and can be used in the XAO analysis. However, the product state needs to be specified or assumed.

XAO analysis of a multi-4*f*-electron system is performed based on the *j*–*j* coupling scheme. The *j* value of each *f* electron is 5/2 or 7/2 and the system is treated as an assembly of such electrons. The 4*f* atomic orbitals for single electrons in a crystal field are calculated as the linear combination of the six or eight basis functions (see Table 1; Tanaka *et al.*, 2008), and 4*f* electrons are allocated to the 4*f* atomic orbitals. In the following discussion *J* values of *p*, *d* and *f* orbitals are attached as a subscript on the right side of each orbital. Fourteen 4*f* states are split into six $4f_{5/2}$ and eight $4f_{7/2}$ states by *j*–*j* coupling. The $4f_{5/2}$ states split further in the O_h crystal field into fourfold Γ_8 and twofold Γ_7 states, and the $4f_{7/2}$ states into twofold Γ_6, fourfold Γ_8 and twofold Γ_7 states. The splitting of the states in crystal fields with lower symmetry was calculated using the program *WAVE*03 and the relationships between the coefficients of the 4*f* atomic orbitals are listed in Table 4 of the paper by Tanaka *et al.* (2008). Ten 5*d* states split into fourfold $5d_{3/2}$ and sixfold $5d_{5/2}$ states by *j*–*j* coupling and $5d_{5/2}$ splits further into fourfold Γ_8 and twofold Γ_7 in the O_h crystal field. Electrons are allocated to these orbitals properly at the first stage of the refinement. The parameters to be refined are populations, κ parameters, which express the expansion ($\kappa < 1$) or contraction ($\kappa > 1$) of the atomic orbital in the crystal field, and the coefficients of each atomic orbital which are refined to fit to the observed EDD. Hereinafter these parameters are called orbital parameters. In the present study the coefficients of the atomic orbitals are fixed by the point-group symmetry of Sm.

Since X-ray diffraction does not measure spins of electrons, terms arising as products of the angular momentum and spins of electrons do not make a difference in the X-ray scattering factors. As an example it was shown that the 3*d*-electron configuration $t_{2g}^2 e_g^1$ has ten terms when spins are taken into account (Kamimura *et al.*, 1969), but the scattering factors of

them are equal (Tanaka *et al.*, 2008). t_{2g} and e_g orbitals are eigenfunctions of a *d* electron in the cubic O_h crystal field. The example just cited indicates that the EDD is expressed as a superposition of the EDD of *d* or *f* electrons with proper *l* or *j* values in a crystal field. The process just stated neglects electron correlation. In the XAO analysis we can skip the tedious derivation of the basic product states.

The valence of Sm in SmB_6 is reported to fluctuate between divalent Sm^{2+} and trivalent Sm^{3+}. The ratio of Sm^{3+} and Sm^{2+} is nearly temperature-independent and established to be $\sim$ 3:7 or 4:6 by measuring the Mössbauer isomer shift (Cohen *et al.*, 1970), ^{11}B NMR (Takigawa *et al.*, 1981), X-ray absorption at the L_{III} edge (Tarascon *et al.*, 1980), and by calculating the lattice constant (Menth, Buehler & Geballe, 1969). SmB_6 is also known to have a narrow band gap at low temperature (Nickerson *et al.*, 1971), which was found by the measurements of resistivity (Menth, Buehler & Geballe, 1969; Allen *et al.*, 1979), Hall effect, magnetic susceptibility and so on. The size of the gap was 50 K (= 4.3 meV) measured by NMR (Takigawa *et al.*, 1981) and ESR (Al'tshuler *et al.*, 1986). It was also measured to be 5.5 meV by the far-IR reflectivity (Travaglini & Wachter, 1984). It was obtained as 27 meV by an LSDA + *U* (LSDA = local spin-density approximation) band calculation (Antonov *et al.*, 2002). However, the detailed EDD and electron configuration of Sm have not yet been determined. The aim of the present study is to measure the EDD of an SmB_6 single crystal by X-ray diffraction at 100, 165, 230 and 298 K, and reveal the electron configuration of SmB_6 by XAO analysis. The properties cited above will be made clear from the EDD and electron configuration.

2. Experimental

Crystal data and experimental conditions are summarized in Table 1. The crystal was shaped into a sphere by the Bond method (Bond, 1951) and the radius was magnified 500 times under a telescope and recorded by a CCD camera. The experimental condition is almost the same as that employed in the EDD measurement of CeB_6 (Tanaka & Ōnuki, 2002). Diffraction intensities for SmB_6 were measured at four temperatures (100, 165, 230 and 298 K) with Mo $K\alpha$ radiation using the four-circle diffractmeter (BRUKER AXS). The orientation matrix of the crystal was determined using {336}, {444} and {155} reflections with 2θ around 75°, where $K\alpha_1$ and $K\alpha_2$ radiations are clearly separated. In order to obtain reliable displacement parameters, time spent measuring higher-order weak reflections was more than ten times longer than that spent for lower-order strong reflections. Since the effect of multiple diffractions on the intensity easily exceeds 1% (Tanaka & Ōnuki, 2002), it was avoided by rotating the crystal around the scattering vector (ψ rotation; Tanaka & Saito, 1975; Tanaka *et al.*, 1994). The optimum ψ angles were calculated using the program *IUANGLE* (Tanaka *et al.*, 1994).

3. Refinement

Relativistic radial functions of Sm^{3+} calculated with the program *HEX* (Liberman *et al.*, 1971) and non-relativistic ones for $B^{0.5-}$ calculated by Mann (1968) were transferred to scattering factors with the program *SFSCF* (programmed by Kiyoaki Tanaka, see also Tanaka & Ōnuki, 2002). The radial functions of the same sub-shell, such as $4f(j = 5/2)$ and $4f(j = 7/2)$ calculated by *HEX*, are almost the same as each other.

At first five 4*f* electrons were allocated equally to the fourfold degenerate $4f_{5/2}\Gamma_8$ and the twofold degenerate Γ_7 orbitals in the O_h crystal field. When the peaks on the difference density map due to 4*f* electrons were not explained with the electrons in the $4f_{5/2}$ orbitals, $4f_{7/2}\Gamma_6$, Γ_8 and Γ_7 orbitals, and 5*d* orbitals were tested.

In order to analyze the electron configuration, XAO analysis (Tanaka *et al.*, 2008) was applied. In the XAO analysis the electron density of each atom was divided into those of core and valence electrons, and the valence ones were further divided into those of sub-shell electrons. The atomic orbitals (AOs) $\Psi_i(\kappa_i \mathbf{r})$ of the valence electrons were expressed as a linear combination of $\psi_i(\kappa_i \mathbf{r})$, which were *s*-, *p*-, *d*- or *f*-orbital functions, in the following way

$$\Psi_i(\kappa_i \mathbf{r}) = \sum_k a_{ik} \psi_k(\kappa_i \mathbf{r}). \qquad (1)$$

The parameter κ_i which expresses the expansion ($\kappa < 1$) and contraction ($\kappa > 1$) of each atomic orbital (AO), as well as the number of electrons $n(Y)$ on an atomic orbital *Y*, are adjustable parameters in the refinement. The κ_i and $n(Y)$ parameters of the degenerate orbitals were constrained to be the same. The coefficients a_{ik} were refined under the orthonormal constraint between the atomic orbitals (Tanaka, 1988). In the present study a_{ik}s were fixed because of the O_h symmetry of the crystal field. The basis functions $\psi_k(\kappa_i \mathbf{r})$ are summarized in Table 1 of the paper by Tanaka *et al.* (2008). Each set of sub-shell orbitals of each atom was treated as an independent 'atom' sharing the coordinates and temperature factors of the nucleus. The change in units of X-ray scattering from an atom to groups of 'sub-shell atoms' makes it possible to handle the non-stoichiometric compounds or solid solutions while keeping the unit cell electrically neutral. In the present study the valence orbitals of Sm were divided into $5p_{1/2}$, $5p_{3/2}$, $4f_{5/2}$, $4f_{7/2}$, $5d_{3/2}$, $5d_{5/2}$ and those of B into $2s$, $2p_x (= 2p_y)$ and $2p_z$. The unit cell was maintained to be electrically neutral by

$$\begin{aligned} &g_{\mathrm{Sm}}[50 + 4n(5p_{3/2}) + 4n(4f_{5/2}\Gamma_8) + 2n(4f_{5/2}\Gamma_7) + 4n(4f_{7/2}\Gamma_8) \\ &+ 2n(4f_{7/2}\Gamma_7) + 4n(5d_{3/2}\Gamma_8) + 4n(5d_{5/2}\Gamma_8) + 2n(5d_{5/2}\Gamma_7)] \\ &+ g_{\mathrm{B}}[2 + n(2s) + 2n(2p_x) + n(2p_z)] = g_{\mathrm{Sm}} Z_{\mathrm{Sm}} + g_{\mathrm{B}} Z_{\mathrm{B}}, \end{aligned} \qquad (2)$$

where g_X and Z_X are the multiplicity and atomic number of the atom *X*. The numbers in front of the electron populations are the degeneracy of each orbital. The constraint was kept throughout the refinement in the present study. Since the B atom was located on the fourfold axis, the $2p_x$ orbital was equivalent to the $2p_y$ orbital, and the $2p_x$ and $2p_y$ orbitals of B are written hereinafter as $2p_{x,y}$.

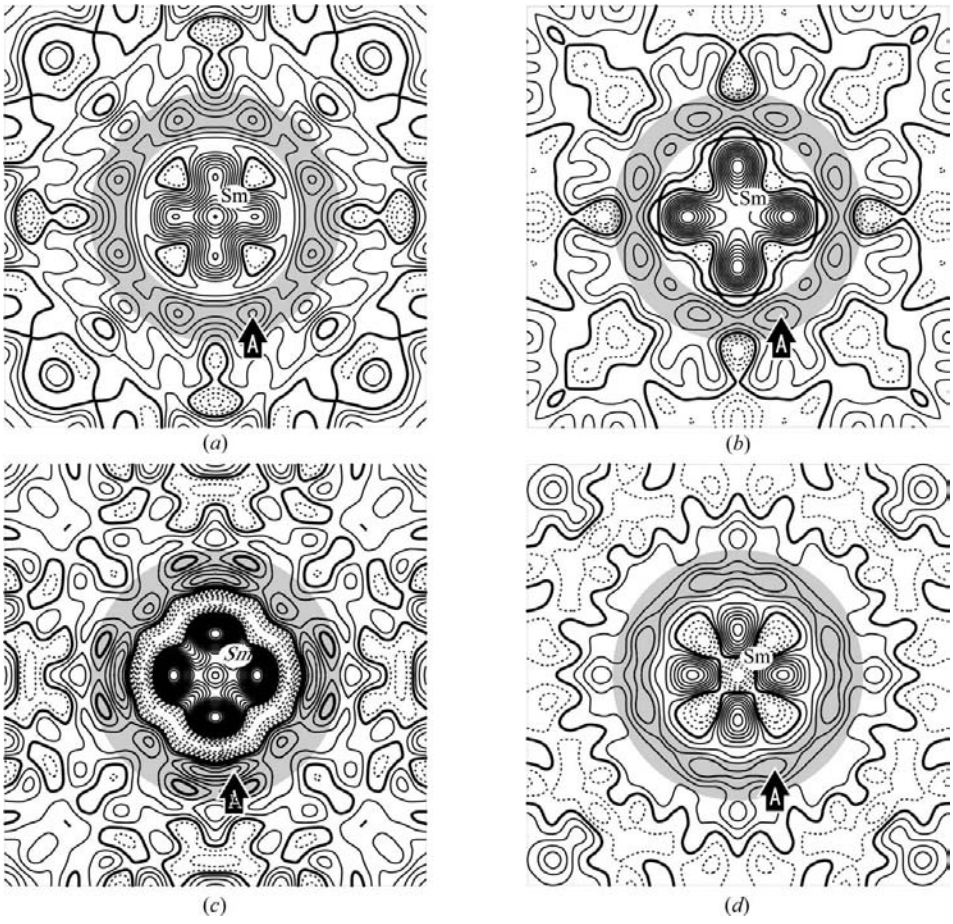

Figure 1
Difference density around Sm at $(\frac{1}{2}, \frac{1}{2}, \frac{1}{2})$ after spherical-atom refinement. (*a*), (*b*), (*c*) and (*d*) are at 100, 165, 230 and 298 K, respectively. The shadow specifies roughly the area of the 5*d* peaks (see text). Contours are at intervals of 0.1 e Å^{-3}. Zero contours are drawn with thick lines, positive and negative contours are drawn with thin and broken lines. The arrow A indicates peak *A* (see text).

Since the orthonormal condition between the AOs and the electrically neutral unit cell are kept strictly in the refinement and the physical significance of each parameter is quite clear, the electron populations obtained are reliable and the parameter interaction in the refinement of a system with heavily condensed electrons like SmB_6 can be minimized. These are important advantages of the XAO analysis. Since two-centre electrons are not treated in the XAO analysis, peaks in the middle of the B—B bonds, which are mainly due to the two-centre electrons, are not expressed well. However, the total number of electrons of the two-centre peaks is very small in SmB_6. The XAO analysis applied to crystals with heavy atoms is expected to give reliable results which can be easily correlated to theories of chemical bonds and band theory.

However, since the orbital parameters and the anharmonic vibration (AHV) parameters are all correlated to the aspherical EDD, it was always a problem to select the parameter to be added at each further stage of the refinement. The difference density was always calculated and the parameter correlated to the largest peak was added since it contributes most to reducing the differences between observed and calculated structure factors. When minor parameters were refined prior to the major ones, the least-squares refinement did not work well. Therefore, the electron populations of AOs were first refined following the process stated in §3.2 and a rough electron configuration was determined. Then κ of the occupied orbitals were added in the refinement. The refinements of the orbital parameters prior to the AHV parameters and the reverse-order refinement did not result in significantly different values, since they were refined together in the final stage of the refinement. The refinement continued as long as the *R* factors were reduced, no matter how small the reduction. However, when the parameter interactions were neglected the change in the hierarchy of parameters sometimes gave different results. There actually were parameter interactions between the orbital parameters, the harmonic temperature factors and anharmonic ones. They were avoided by fixing one of the parameters alternately.

3.1. Refinement of the spherical-atom model

In the spherical-atom model, five 4*f* electrons were initially allocated equally to the $4f_{5/2}\Gamma_8$ and Γ_7 orbitals to make the EDD around the atom spherical. No electrons were assigned to the 5*d*, $4f_{7/2}$ and the 6*s* orbitals of Sm^{3+} at this stage. The 2*s* and 2*p* orbitals of the $B^{0.5-}$ ion were assumed to have 2.0 and 0.5 electrons. Then the scale factor, atomic coordinates, harmonic temperature factors, and isotropic and anisotropic Type I extinction parameters were refined consecutively. Dispersion terms were taken from the *International Tables for Crystallography* (1992, Vol. C) and Type I extinction (Becker & Coppens, 1974*a*,*b*, 1975) with a Thornley–Nelmes distribution function (Thornley & Nelmes, 1974) was assumed. The difference density obtained after this stage can be taken to be experimental, expressing the aspherical features of EDD, since no modification to the aspherical electron density owing

to models of atomic orbitals is included and the orbital functions used were well known. The difference density around Sm and B atoms after spherical-atom refinement is illustrated in Figs. 1 and 2.

3.2. XAO analysis of 4*f*- and 5*d*-EDD and anharmonic vibration (AHV)

In this stage the populations $n(Y)$ and κ_i of the valence orbitals were refined. The ground state of the Sm^{3+} ion in free space does not have 5*d* and 6*s* electrons. However, since the $5d_{5/2}$ orbitals of CeB_6 were occupied above room temperature (Makita *et al.*, 2007, 2008), electron populations of $4f_{5/2}$, $4f_{7/2}$, $5d_{3/2}$, $5d_{5/2}$ and $6s_{1/2}$ orbitals were also refined in SmB_6. Starting from the electron configurations of $[Xe]4f_{5/2}^5$ for Sm and $[He](2s)^2(2p_x)^{1/2}(2p_y)^{1/2}(2p_z)^{1/2}$ for B, the populations of the orbitals just mentioned were first refined keeping the unit cell electrically neutral. When a population becomes negative or exceeds its limit, 1 for the spin-orbital of Sm and 2 for orbitals of B, it is fixed to the limiting value. The populations of 6*s* and $5d_{3/2}$ were refined, but they were not occupied throughout the refinement. The populations of fourfold degenerate $5p_{3/2}$ orbitals always exceeded 1, so they were fixed to 1. Since the four $5p_{3/2}$ orbitals are restricted to be equally occupied by the crystal symmetry, their EDD is spherical as a whole and does not contribute to the aspherical features of the difference-density maps. However, the κ parameters were refined including those of the $5p_{3/2}$ orbitals, since it was the outermost closed-shell orbital of Xe and easily affected by the crystal field. The doubly degenerate $5p_{1/2}$ orbitals were not refined, since they always caused an abnormal fluctuation in the refinement and thus were taken as part of the core orbitals.

The AHV parameters were refined using the method of Tanaka & Marumo (1983) after populations and κ parameters were refined. AHV parameters are restricted by the site symmetry of Sm(*m*3*m*) and B(4*mm*), and the anharmonic potential V of each atom is represented by the following equation

$$V_{\rm Sm} = q_{1111}\left(u_1^4 + u_2^4 + u_3^4\right) + q_{1122}\left(u_1^2u_2^2 + u_1^2u_3^2 + u_2^2u_3^2\right), \quad (3)$$

$$V_{\rm B} = c_{111}\left(u_1^3 + u_2^3\right) + c_{333}u_3^3 + q_{1111}\left(u_1^4 + u_2^4\right) + q_{3333}u_3^4 + q_{1122}u_1^2u_2^2 + q_{1133}\left(u_1^2u_3^2 + u_2^2u_3^2\right), \quad (4)$$

where $\boldsymbol{u} = (u_1, u_2, u_3)$ is a displacement vector from the equilibrium position of each atom defined on the Cartesian coordinates with axes parallel to the crystal axes ***a***, ***b*** and ***c***. Since AHV parameters are closely related to high-order reflections, 4*f* electrons located near the inner shell are expected to be strongly affected by AHV. In the previous study (Tanaka & Ōnuki, 2002), a significant shift of the *z* coordinate was observed when the anharmonic cubic parameters were refined with the *z* coordinate. Such a shift was also observed in the present study.

The interaction between harmonic and anharmonic parameters was always severe and they were refined alternately. The interactions between the parameters of Sm are those between the populations of $4f_{5/2}\Gamma_8$ and $4f_{7/2}\Gamma_6$, κ of $4f_{5/2}\Gamma_8$ and $4f_{5/2}\Gamma_7$, and AHV parameters of q_{1111} and q_{1122}. Correlations for the B atom were observed between the population and κ of $2p_{x,y}$, and between AHV parameters of c_{111} and c_{333}, q_{1111} and q_{1122}, q_{1133} and q_{3333}. To avoid these correlations they were refined alternately. Each refinement process is explained in the following paragraphs.

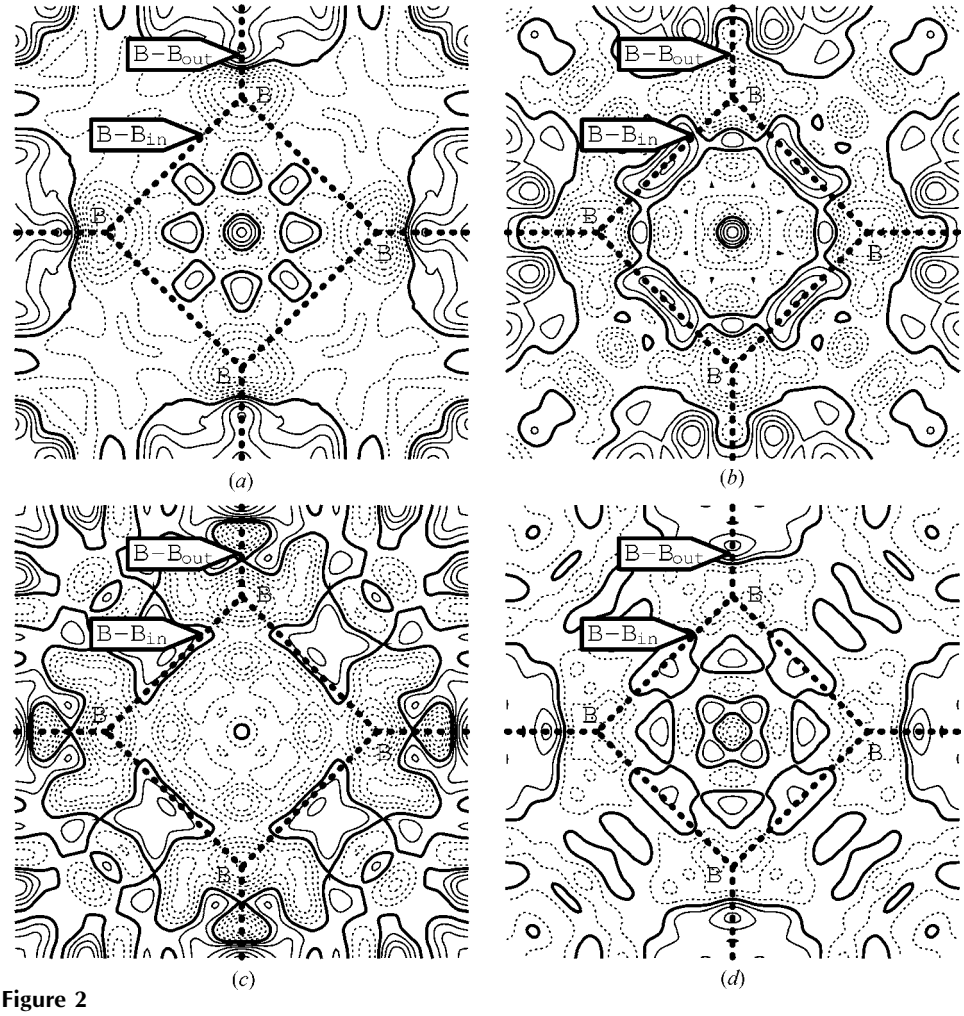

Figure 2
Difference densities around B_6 on the $z = 0$ plane after spherical-atom refinement. (*a*), (*b*), (*c*) and (*d*) are at 100, 165, 230 and 298 K, respectively. Contours are as in Fig. 1.

3.2.1. Refinement (I) of $4f_{5/2}\Gamma_7$ and Γ_8 orbitals. The aspherical EDD was refined in three steps, avoiding the parameter interactions wherever possible. When the interactions could not be avoided, the interacting parameters were refined as just described. The difference-density maps were calculated after each step and the possible parameters of the atomic orbital to be refined were introduced taking into account the characteristic shape of each orbital in Fig. 3. Fig. 3(*a*) illustrates the shape of the sum of the EDD of the fourfold $4f_{5/2}\Gamma_8$ orbitals normalized to the EDD of one electron. It elongates along ⟨100⟩ directions equally in SmB_6. The $4f_{5/2}\Gamma_7$ orbital in Fig. 3(*b*) extends along ⟨111⟩ and ⟨110⟩. The $4f_{7/2}\Gamma_6$ orbitals extend along ⟨100⟩, as illustrated in Fig. 3(*c*). The radial distribution functions of $5p_{3/2}$, $4f_{7/2}$ and $5d_{5/2}$ of Sm, and that of 2*p* of B are shown in Fig. 4. In order to demonstrate how widely the Sm-5*d* and B-2*p* orbitals are overlapped, the origin of the radial function of B-2*p* was placed at 3.04 Å, which is the Sm—B bond length, and it is drawn from there to the opposite direction to those of the orbitals of Sm. It is evident that the B-2*p* and Sm-5*d* orbitals overlap very well. The third peak position of the radial distribution function of Sm-5*d* was located around 1 Å.

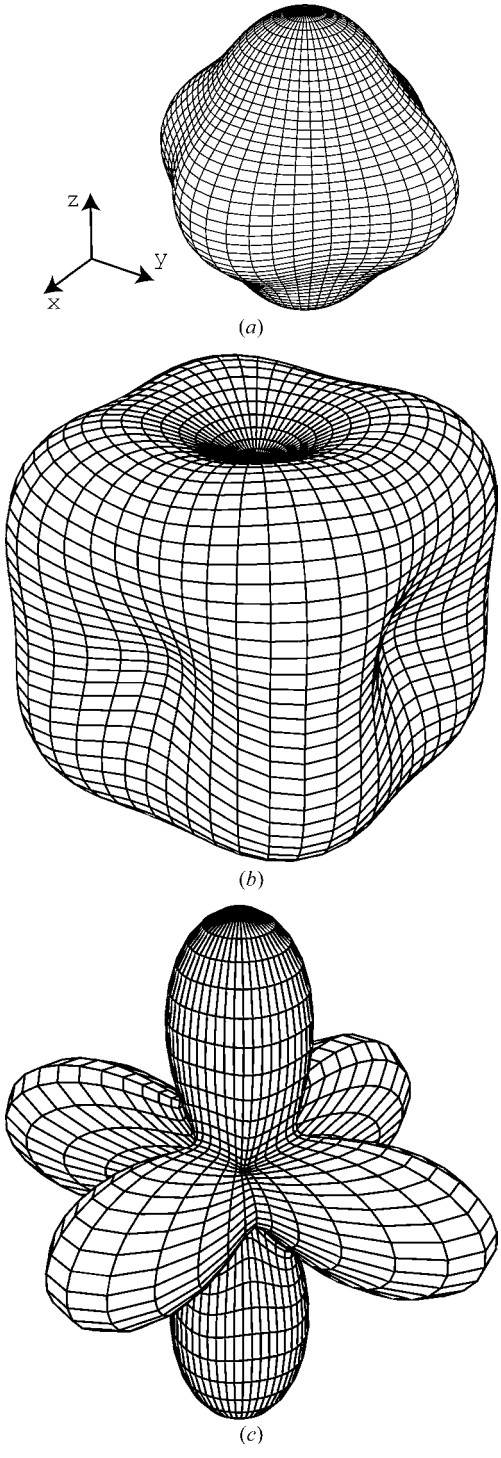

Figure 3
Schematic drawing of the EDD (*a*) of the sum of $4f_{5/2}\Gamma_8$ orbitals, (*b*) of $4f_{5/2}$ Γ_7 and (*c*) of $4f_{7/2}\Gamma_6$ orbitals. $5d_{5/2}\Gamma_6$ orbitals extend in the same directions as those of $4f_{5/2}\Gamma_8$.

Sm-$4f_{5/2}\Gamma_8$, Γ_7, Sm-$5p_{3/2}$, B-2*s* and B-2*p* valence orbitals were refined first. All the electron populations and κ values of these orbitals were refined. As stated earlier, when a population exceeded its quantum mechanical limit, it was fixed to the limiting value and was not refined to avoid useless parameter interactions. Since the selection of the population parameters as variables was carried out in an earlier stage of the refinement, it was occasionally refined later to assess whether it actually had the limiting value. Since $n(2s)$ first exceeds 2.0 and $n(5p_{3/2})$ exceeds 1.0, they were fixed to 2.0 and 1.0. $n(2p_z)$ was used as an adjustable parameter to keep the electrical neutral condition (2) and was not refined. However, all the derivatives of the other parameters in (2) are expressed in terms of those of themselves and of $n(2p_z)$. Therefore, $n(2p_z)$ can be said to be refined with the other parameters in (2) (see Appendix C of Tanaka *et al.*, 2008). The κ parameters were then refined and the results are listed in Table 2. The populations of the $4f_{5/2}\Gamma_8$ orbitals always tended to exceed 1 at 165 and 230 K, and were fixed to 1. The B-2*s* orbital is fully occupied but some of the 2*p* electrons of B are transferred to Sm. The residual density after refinement (I) is illustrated in Fig. 5.

3.2.2. Refinement (II) of $4f_{7/2}\Gamma_6$ orbitals. Since the peaks near Sm still remain along ⟨100⟩ in Figs. 5(*b*) and (*c*) at 165 and 230 K, $n(4f_{7/2}\Gamma_6)$, $n(4f_{7/2}\Gamma_8)$ and $n(4f_{7/2}\Gamma_7)$ are then added as unknown parameters to the refinement with the starting values of 0. The $4f_{7/2}\Gamma_6$ orbitals which extend along ⟨100⟩ were calculated to be the most stable among the $4f_{7/2}$ orbitals using the program *HEX* (Liberman *et al.*, 1971). The populations of $4f_{7/2}\Gamma_8$ and $4f_{7/2}\Gamma_7$ with higher energy than $4f_{7/2}\Gamma_6$ were always less than 0 and excluded from the refinement. In refinement (II) there are very large correlations between the populations and κ parameters of $4f_{5/2}\Gamma_8$ and $4f_{7/2}\Gamma_6$. It seems to be due to the similar direction of extension of the two orbitals, which were refined alternately. $n(4f_{7/2}\Gamma_6)$ is significant at 165, 230 and 298 K, but at 100 K $4f_{7/2}\Gamma_6$ would not be occupied. This is very interesting and will be discussed in the forthcoming section. Accordingly, only the residual densities at 165, 230 and 298 K are presented in Figs. 6(*a*), (*b*) and (*c*). The parameters after refinement (II) are listed in Table 3.

3.2.3. Refinement (III) of $5d_{5/2}\Gamma_8$ orbitals. The 5*d* sub-shell of Sm is expected to split into $5d_{3/2}$ and $5d_{5/2}$ with the spin-orbit interaction. The $5d_{3/2}\Gamma_8$ orbitals do not split, but the $5d_{5/2}$ orbitals split into the fourfold Γ_8 and twofold Γ_7 orbitals. The shapes of the $5d_{5/2}\Gamma_8$ and Γ_7 orbitals are exactly the same as the corresponding ones of the $4f_{5/2}$ orbitals except for the size of the orbitals. The fourfold $5d_{3/2}\Gamma_8$ orbitals form a spherical EDD since they are degenerate and electrons are allocated equally to the four orbitals. The $5d_{3/2}\Gamma_8$ and $5d_{5/2}\Gamma_7$ orbitals were reduced to t_{2g} orbitals and the $5d_{5/2}\Gamma_8$ orbitals to e_g orbitals when the spin–orbit interaction was neglected. The shaded areas around 1 Å from Sm in Figs. 1, 5, 6 and 7 show the 5*d* area. In our previous study on CeB_6 above room temperature it was shown that 5*d* peaks appear in the area $\sim$ 0.8–0.9 Å from Ce (Makita *et al.*, 2008). The positive peak *A* at $\sim$ 1.00 Å from Sm in Fig. 5(*a*) at 100 K and in Fig. 6(*c*) at 298 K are higher than those at an intermediate temperature of 165 and 230 K in Figs. 6(*a*) and (*b*). In order to explain these peaks, the electron populations of $5d_{3/2}\Gamma_8$, $5d_{5/2}\Gamma_8$ and Γ_7 orbitals were added in the refinement. However, the populations of the $5d_{3/2}\Gamma_8$ and $5d_{5/2}\Gamma_7$ orbitals, as well as that of the 6*s* orbital, always became less than 0 and were fixed to 0, the reason for which will be discussed in the next section. The κ parameters of the $5d_{5/2}\Gamma_8$ orbitals were then refined. It was also noted that the parameter interaction between the populations of B-$2p_{x,y}$ and $5d_{5/2}\Gamma_8$ was severe. The results are listed in Table 3 and the final residual densities are illustrated in Fig. 7.

4. Results and discussion

4.1. Observed aspherical EDD after spherical-atom refinement

In the spherical-atom refinement the fourfold $4f_{5/2}\Gamma_8$ and twofold Γ_7 orbitals are allocated 5/6 electrons equally to make the 4*f*-EDD spherical. Therefore, unmodified anisotropic characteristics of the observed EDD are displayed in Figs. 1 and 2. The residual density around Sm is positive as a whole, as illustrated in Fig. 1, and that around B is negative, see Fig. 2. It indicates that Sm and B_6 are closer to neutral and have more and less electrons than their formal valences 3+ and 3−, respectively. There are positive peaks along the ⟨100⟩ direction 0.3 Å from Sm at the centre of Figs. 1(*a*)–(*d*) with heights of 0.81, 1.08, 1.88 and 0.74 e Å^{-3}. Since the $4f_{5/2}\Gamma_8$ or $4f_{7/2}\Gamma_6$ orbitals extend along ⟨100⟩, as illustrated in Fig. 3, these orbitals were expected to be more occupied than $4f_{5/2}\Gamma_7$ extending along ⟨111⟩ and ⟨110⟩ (see Fig. 3*b*). Since the $4f_{7/2}\Gamma_6$ orbitals have higher energy than the $4f_{5/2}\Gamma_8$ orbital, $n(4f_{7/2}\Gamma_6)$ is expected to be smaller than $n(4f_{5/2}\Gamma_8)$. On the other hand, the negative peaks or areas along ⟨110⟩ directions at $\sim$ 0.3–0.5 Å from Sm in Figs. 1(*a*)–(*d*) are explained by less occupation of $4f_{5/2}\Gamma_7$ orbitals than 5/6 after refinement (I) in Table 2. The positions of these peaks correspond to the area around the highest position of the 4*f* radial distribution functions in Fig. 4 calculated by *HEX* (Liberman *et al.*, 1971).

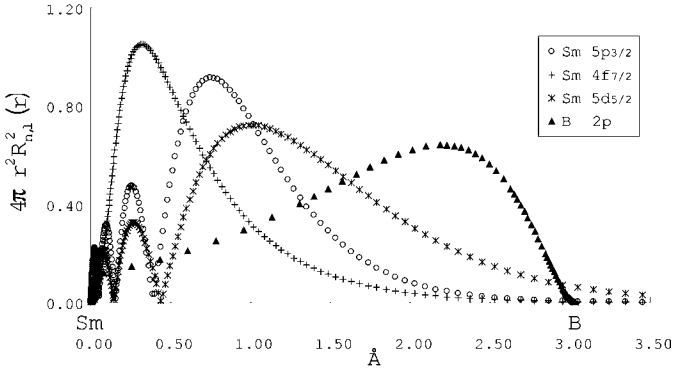

Figure 4
Radial distribution function of Sm-$4f_{7/2}$, $5p_{3/2}$, $5d_{5/2}$ and B-2*p* orbitals. $4f_{5/2}$ and $4f_{7/2}$, $5d_{3/2}$ and $5d_{5/2}$ orbitals have approximately the same radial distribution functions, respectively.

4.2. XAO analysis of 4*f*-EDD

As stated in §3.2.1, $4f_{5/2}\Gamma_8$ orbitals are fully occupied at 165 and 230 K. They are also fully occupied within experimental error at 100 and 298 K, although $n(4f_{5/2}\Gamma_8)$ did not exceed 1.0 in the refinement. Twofold degenerate $4f_{5/2}\Gamma_7$ orbitals are partially occupied. The numbers of 4*f* electrons at this stage of the refinement are 4.7 (6), 5.0 (2), 4.7 (3) and 4.3 (2) K at 100, 165, 230 and 298 K. The peaks along ⟨100⟩ around the centre of Fig. 1 are reduced or deleted in Fig. 5 after refinement (I) analyzed the two kinds of $4f_{5/2}$ orbitals. However, the peaks along the ⟨100⟩ directions with heights of 0.49 and 0.79 e Å^{-3} at 165 and 230 K in Fig. 5 are still very high, although refinement (I) reduced the peaks from 1.08 and 1.88 e Å^{-3} to less than half their initial values. This indicates that further refinement of the orbital extending along ⟨100⟩ is necessary. Accordingly, the parameters of the doubly degenerate $4f_{7/2}\Gamma_6$ orbitals which extend along ⟨100⟩, as shown in Fig. 3(*c*), were added in refinement (II). It was revealed that the $4f_{7/2}\Gamma_6$ orbitals were occupied at 165 and 230 K, reducing the peaks to 0.38 and 0.18 e Å^{-3} in Figs. 6(*a*) and (*b*), accompanied by the reduction of *R* factors, which showed that refinement including $4f_{7/2}\Gamma_6$ orbitals was necessary. It is very interesting that $4f_{7/2}\Gamma_6$ orbitals were not occupied at 100 K, which will be discussed later.

4.3. XAO analysis of 5*d* electrons

When the crystal field of Sm is formed by the negatively charged B_6 octahedra with their centres at the corners of the cubic unit cell, the energy of the $5d_{3/2}$ states is the lowest among the 5*d* orbitals. However, the 5*d* electrons did not occupy the $5d_{3/2}\Gamma_8$ and $5d_{5/2}\Gamma_7$ orbitals, which stem from 5*d*-t_{2g} orbitals in the strong-field model, but the $5d_{5/2}\Gamma_8$ orbitals which correspond to 5*d*-e_g orbitals were occupied. This indicates that the O_h crystal field was inverted by electron transfer from B to Sm and the $5d_{5/2}\Gamma_8$ states lie lower, as illustrated in Fig. 4 of the paper by Makita *et al.* (2007). It was reported that the conduction band of LaB_6 is mainly composed of 5*d*-e_g electrons (Harima, 1988), which is the $5f_{5/2}\Gamma_8$ orbital in the present study. The energy level of the atomic orbital B-2*p* is

Table 2
Parameters after spherical-atom refinement and refinement (I).

Parameters for B at (0,0,z). Electron populations n, kappa parameter κ, anisotropic displacement factors U^{ij} ($\times 10^{-5}$ Å^2), harmonic b_i ($\times 10^{-19}$ J Å^{-2}), anharmonic cubic c_{iij} ($\times 10^{-19}$ J Å^{-3}) and quartic parameters q_{iiij} ($\times 10^{-19}$ J Å^{-4}) and the degeneracy d of orbitals are listed. Significant c_{iij} and q_{iiij} are written in bold letters. The height of $\Delta\rho$ (peak A; e Å^{-3}) is listed. Anisotropic temperature factors are defined as $T_H = \exp(-2\pi^2 \sum_{i,j} h_i h_j a_i^* a_j^* U_{ij})$. Anharmonic potentials V are defined in the text. $R_1 = \sum \big||F_o| - |F_c|\big| / \sum |F_o|$, $R_2 = \sum \big(|F_o| - |F_c|\big)^2 / \sum |F_o|^2$. Anisotropic type I extinction parameters ($\times 10^4$s) are given with the Thornley–Nelmes distribution function. For details of the refinements, see text in §3.

		Spherical model refinement				Aspherical model refinement (I)			
	d	100 K	165 K	230 K	298 K	100 K	165 K	230 K	298 K
R_1		0.01014	0.00876	0.01164	0.00897	0.00938	0.00832	0.01051	0.00789
R_2		0.00993	0.00901	0.01274	0.00888	0.00920	0.00864	0.01167	0.00787
Sm									
U^{11}		312 (2)	419 (4)	570 (2)	750 (2)	304 (2)	410 (6)	570 (3)	763 (2)
b_1		4.43 (3)	5.44 (5)	5.57 (2)	5.49 (1)	4.54 (3)	5.55 (8)	5.57 (3)	5.39 (1)
$n(5p_{3/2})$	4	1.00	1.00	1.00	1.00	1.00	1.00	1.00	1.00
$\kappa(5p_{3/2})$		1.00	1.00	1.00	1.00	0.89 (4)	0.86 (4)	0.74 (5)	0.83 (2)
$n(4f_{5/2}\Gamma_8)$	4	5/6	5/6	5/6	5/6	0.95 (8)	1.00	1.00	0.99 (2)
$\kappa(4f_{5/2}\Gamma_8)$		1.00	1.00	1.00	1.00	0.99 (2)	0.99 (3)	1.01 (3)	0.95 (1)
$n(4f_{5/2}\Gamma_7)$	2	5/6	5/6	5/6	5/6	0.45 (12)	0.52 (12)	0.34 (15)	0.19 (5)
$\kappa(4f_{5/2}\Gamma_7)$		1.00	1.00	1.00	1.00	1.10 (9)	1.31 (17)	1.04 (20)	1.03 (4)
q_{1111}		0.00	0.00	0.00	0.00	**1.14 (52)**	**2.71 (9)**	**0.32 (22)**	**0.26 (9)**
q_{1122}		0.00	0.00	0.00	0.00	−1.22 (154)	**−4.77 (47)**	−0.35 (80)	**0.57 (24)**
Sm valence		+3.00	+3.00	+3.00	+3.00	+3.30 (40)	+2.96 (20)	+3.32 (30)	+3.66 (13)
$\Delta\rho$ (peak A)		+0.61	+0.43	+0.43	+0.49	+0.47	+0.29	+0.25	+0.32
B									
z		0.3003 (2)	0.3001 (2)	0.3001 (2)	0.3003 (1)	0.2992 (3)	0.2963 (3)	0.2989 (2)	0.2983 (1)
U^{11}		377 (11)	424 (10)	470 (11)	516 (6)	391 (10)	419 (9)	481 (10)	549 (5)
U^{33}		282 (17)	270 (14)	291 (16)	365 (8)	247 (16)	256 (13)	275 (15)	365 (7)
$b1$		3.67 (11)	5.51 (12)	6.77 (15)	7.98 (9)	3.53 (9)	5.44 (12)	6.60 (14)	7.49 (7)
$b2$		4.90 (28)	8.58 (40)	10.9 (6)	11.3 (3)	5.59 (4)	8.92 (45)	11.5 (6)	11.2 (2)
$n(2s)$	1	2.00	2.00	2.00	2.00	2.00	2.00	2.00	2.00
$\kappa(2s)$		1.00	1.00	1.00	1.00	1.06 (4)	0.84 (5)	0.94 (5)	0.97 (2)
$n(2p_x(=2p_y))$	2	1/2	1/2	1/2	1/2	0.42 (7)	0.40 (6)	0.49 (8)	0.45 (2)
$\kappa(2p_x(=2p_y))$		1.00	1.00	1.00	1.00	0.49 (4)	0.68 (9)	070 (10)	0.52 (2)
$n(2p_z)$	1	1/2	1/2	1/2	1/2	0.71 (16)	0.67 (13)	0.58 (17)	0.70 (6)
$\kappa(2p_z)$		1.00	1.00	1.00	1.00	0.91 (14)	0.97 (17)	0.96 (24)	0.87 (4)
c_{311}		0.00	0.00	0.00	0.00	**5.04 (481)**	**−12.8 (55)**	−5.46 (612)	**−4.45 (243)**
c_{333}		0.00	0.00	0.00	0.00	−8.89 (1017)	−6.93 (1360)	−2.68 (1535)	**−5.27 (428)**
q_{1111}		0.00	0.00	0.00	0.00	0.66 (204)	1.21 (341)	−1.27 (281)	**−2.20 (108)**
q_{3333}		0.00	0.00	0.00	0.00	2.10 (732)	**−30.1 (220)**	−9.09 (1269)	**−10.6 (37)**
q_{1122}		0.00	0.00	0.00	0.00	−4.52 (661)	−1.43 (815)	5.12 (822)	**10.7 (35)**
q_{1133}		0.00	0.00	0.00	0.00	−1.56 (1314)	11.3 (247)	7.41 (2018)	**12.5 (63)**
Extinction									
Y_{11}		28.4 (50)	41.2 (51)	25.4 (66)	19 (1)	39.9 (66)	56.1 (65)	23.0 (67)	26.9 (11)
Y_{22}		19.8 (26)	15.0 (47)	20.7 (43)	25 (1)	22.6 (31)	23.0 (63)	26.2 (60)	35.0 (8)
Y_{33}		19.7 (10)	27.1 (14)	40.1 (27)	39 (1)	23.0 (12)	32.7 (13)	49.2 (43)	62.5 (22)
Y_{12}		−5.7 (24)	−6.9 (34)	−13.6 (51)	2.0 (5)	−6.05 (293)	−3.47 (469)	−15.3 (57)	3.5 (7)
Y_{13}		1.6 (16)	3.8 (18)	14.2 (28)	−3.5 (7)	1.12 (192)	1.34 (228)	25.0 (32)	−4.9 (10)
Y_{23}		1.3 (11)	3.9 (20)	2.2 (23)	0.4 (6)	1.41 (121)	4.52 (256)	2.27 (290)	−0.8 (9)

−0.61971 a.u. (Mann, 1968) and that of Sm-5d ranges from −1.13 to 1.11 a.u., which is calculated with *HEX* (Liberman *et al.*, 1971). They are the closest among the AOs of B and Sm. Since the B-2p and Sm-5d orbitals overlap well, as illustrated in Fig. 3, and their energy levels are very close, it is natural that the conduction band consists of them. Therefore, the 5d-EDD observed is explained as part of the EDD of the conduction band composed of B-2p and $5d_{5/2}\Gamma_8$ orbitals. It was pointed out by Makita *et al.* (2007, 2008) in a study on CeB_6 that the energy difference of the 2p and 5d states was smaller in CeB_6. Judging from the populations of the relevant orbitals in Table 3, the 5d electrons do not seem to be excited from the 4f states, but are part of the conduction electrons. The inter-band optical spectra of SmB_6 at 300 K measured by Kimura *et al.* (1990) reported that the conduction bands were made mainly by the non-bonding and anti-bonding orbitals of B-2p and Sm-5d orbitals, however, the conduction band was located 5–6 eV above the Fermi level.

Now let us examine the results of the XAO analysis of 5d orbitals. The largest peaks under the shadow named Peak A around the ⟨100⟩ directions remain at ∼ 1.0 Å from Sm in Figs. 1(*a*)–(*d*). The height of Peak A is listed in Tables 2 and 3. They can be ascribed to the 5d orbitals, since similar peaks were also found around Ce in CeB_6 at ∼ 0.8–0.9 Å from Ce in which 5d orbitals were fully occupied at 430 K (Makita *et al.*, 2007) and partially occupied at 340 and 535 K (Makita *et al.*, 2008). The peaks have heights of 0.61 e Å^{-3} at 100 K and 0.43–0.49 e Å^{-3} at the other temperatures after the spherical-atom refinement.

They were reduced after refinement (I) to 0.47 e Å^{-3} at 100 K and 0.25–0.32 e Å^{-3} at the other temperatures in Fig. 5. They remain almost unchanged after refinement (II) with heights of 0.29, 0.27 and 0.30 e Å^{-3} in Fig. 6 at 165, 230 and 298 K. Since the 5*d* orbital is not included in refinements (I) and (II), the reduction of the peaks was achieved mainly by the expansion of the $5p_{3/2}$ orbital (see κ in Tables 2 and 3), which is distributed spherically and is located a little inside the 5*d*-EDD, as illustrated in Fig. 4.

Since the ratio of the valence electrons to the total number of electrons, and the *R* factors after the spherical-atom refinement are very small, the reduction of the *R* factor is also small after the XAO analysis of the aspherical EDD of 5*d* electrons. Furthermore, the averaged EDD of 4*f* is 6.96 times larger than that of 5*d*, since the mean radius of 4*f* and 5*d* orbitals of Sm is 0.901 and 1.72 a.u. (= 0.477 and 0.910 Å; Mann, 1968). Accordingly, reduction by 0.1 e Å^{-3} of the 5*d* peak heights corresponds to a reduction of the 4*f* peaks by 0.70 e Å^{-3}. Therefore, in our previous work (Makita *et al.*, 2008) criteria were proposed to judge the validity of the refinement. Similar criteria are also proposed in the present study. The criteria are the reduction of:

(i) the *R* factors,

(ii) the height of peak *A*,

(iii) the residual density around the B atom, especially the height of the peak at the centre of the B—B bond in the B_6 octhedra, and

(iv) the physical validity.

R factors in Tables 2 and 3 are reduced after each refinement. However, the reduction of *R* factors from refinement (II) to (III) at 230 K is small.

The peak heights were reduced after refinement (III), in which the population and κ parameters of the $5d_{5/2}\Gamma_8$ orbitals were refined. Comparison of Fig. 6(*c*) after refinement (II) to Fig. 7(*d*) after refinement (III) shows a significant reduction of peak *A* from 0.30 to 0.17 e Å^{-3} and the negative 4*f* peaks close to Sm were reduced from −0.23 to −0.13 e Å^{-3} at 298 K. Figs. 5(*a*) and 7(*a*) show the reduction of peak *A* and the peak on Sm from 0.47 to 0.31 e Å^{-3}, and from 0.88 to 0.64 e Å^{-3} at 100 K, respectively, although the peaks at the 4*f* area increased from 0.07 to 0.22 e Å^{-3}. When Fig. 7(*b*) at 165 K is compared with Fig. 6(*a*), the positive and negative peaks were enhanced a little but peak *A* was reduced from 0.29 to 0.20 e Å^{-3}. Comparison of Fig. 6(*b*) to 7(*c*) at 230 K shows deeper negative peaks along ⟨100⟩ in Fig. 7(*c*), but peak *A* was reduced from 0.27 to 0.17 e Å^{-3}. The reduction of peak heights seems to be significant, as discussed earlier. Therefore, it seems proper to deduce that $5d_{5/2}\Gamma_8$ orbitals are occupied.

The resistivity of SmB_6 (shown in Fig. 1 of the paper by Allen *et al.*, 1979) changes smoothly with temperature. Since the 5*d* electrons are the essential part of the conduction band and since the resistivity changes smoothly with temperature, it is more probable that electrons are located at 5*d* orbitals at the four temperatures, although the reduction of *R* factors from refinement (II) to (III) is very small. However, more accurate measurement is desirable for the EDD analysis of the compound with highly condensed electrons such as rare-earth compounds. In our previous study on CeB_6 above room temperature, 5*d* orbitals were also occupied. Recently, the reflection intensities were measured up to $\sin\theta/\lambda$ = 1.37 Å^{-1} at room temperature with the synchrotron radiation beam at BL14 equipped with the avalanche-photodiode detector

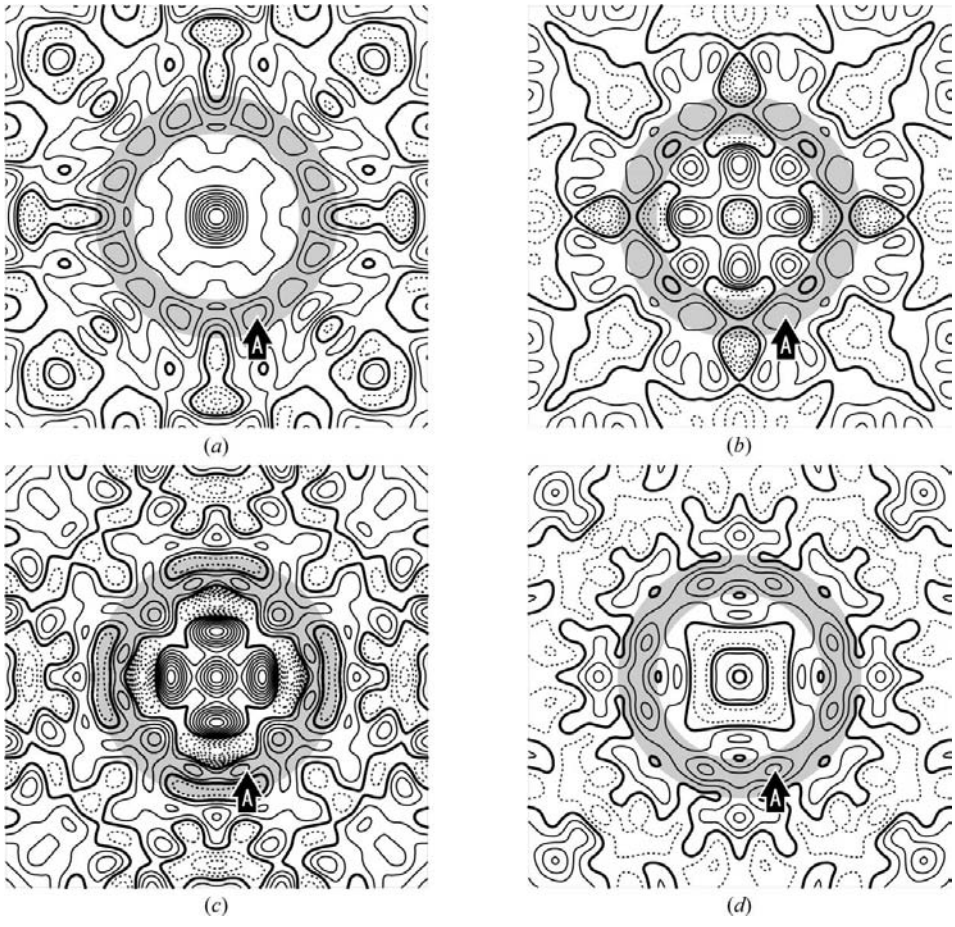

Figure 5
Difference densities around Sm after refinement (I). (*a*), (*b*), (*c*) and (*d*) are at 100, 165, 230 and 298 K, respectively. Contours are as in Fig. 1. Note that the contour level at the border of the shaded circle and that inside in (*a*) is 0.3 e Å^{-3}. The concentric circle around Sm in (*a*) starts from 0.3 e Å^{-3}.

Table 3
Parameters after refinement (II) and refinement (III).

		Aspherical model refinement (II)			Aspherical model refinement (III) (final)			
	d	165 K	230 K	298 K	100 K	165 K	230 K	298 K
R_1		0.00815	0.01036	0.00778	0.00887	0.00793	0.01028	0.00747
R_2		0.00850	0.01153	0.00777	0.00891	0.00837	0.01151	0.00755
Sm								
U^{11}		427 (4)	567 (3)	764 (3)	304 (3)	421 (1)	561 (1)	767 (2)
b_1		5.33 (5)	5.61 (3)	5.38 (2)	4.55 (5)	5.41 (1)	5.66 (7)	5.36 (2)
$n(5p_{3/2})$	4	1.00	1.00	1.00	1.00	1.00	1.00	1.00
$\kappa(5p_{3/2})$		0.82 (4)	0.75 (4)	0.84 (2)	0.87 (4)	0.84 (4)	0.75 (5)	0.85 (1)
$n(4f_{5/2}\Gamma_8)$	4	1.00	1.00	0.69 (3)	0.96 (9)	1.00	1.00	0.77 (3)
$\kappa(4f_{5/2}\Gamma_8)$		0.75 (5)	1.02 (3)	1.09 (3)	0.99 (3)	0.83 (2)	1.00 (3)	1.11 (3)
$n(4f_{5/2}\Gamma_7)$	2	0.56 (10)	0.30 (13)	0.22 (6)	0.48 (12)	0.67 (13)	0.61 (13)	0.59 (7)
$\kappa(4f_{5/2}\Gamma_7)$		1.10 (7)	1.12 (17)	1.01 (12)	1.07 (11)	1.10 (10)	1.04 (8)	0.77 (6)
$n(4f_{7/2}\Gamma_6)$	2	0.46 (15)	0.53 (15)	0.51 (6)	0.00	0.44 (12)	0.59 (13)	0.47 (6)
$\kappa(4f_{7/2}\Gamma_6)$		0.72 (16)	0.84 (21)	0.97 (4)	–	0.95 (9)	0.98 (8)	1.01 (7)
$n(5d_{5/2}\Gamma_8)$	4	0.00	0.00	0.00	1.00	0.75 (24)	0.56 (16)	0.78 (6)
$\kappa(5d_{5/2}\Gamma_8)$		–	–	–	1.07 (9)	1.08 (10)	1.18 (16)	1.04 (4)
$n(5d_{5/2}\Gamma_7)$	2	0.00	0.00	0.00	0.00	0.00	0.00	0.00
$\kappa(5d_{5/2}\Gamma_7)$		–	–	–	–	–	–	–
q_{1111}		**1.03 (55)**	**1.36 (24)**	**1.16 (13)**	**1.0 (7)**	**3.2 (8)**	−0.03 (7)	**0.61 (2)**
q_{1122}		**−2.71 (149)**	**−3.42 (80)**	−0.12 (35)	−1.8 (21)	**−7.8 (26)**	**−0.5 (2)**	**2.08 (6)**
Sm valence		+1.96 (36)	+2.34 (40)	+3.78 (21)	−0.80 (43)	−1.22 (102)	−0.64 (74)	−0.32 (33)
$\Delta\rho$ (peak *A*)		+0.29	+0.27	+0.30	+0.31	+0.20	+0.17	+0.17
B								
z		0.2967 (2)	0.2989 (2)	0.2983 (1)	0.2994 (3)	0.2963 (3)	0.2990 (2)	0.2982 (1)
U^{11}		440 (10)	478 (10)	549 (6)	388 (10)	431 (8)	471 (10)	538 (5)
U^{33}		277 (13)	272 (14)	369 (8)	244 (15)	274 (12)	268 (16)	368 (7)
b_1		5.18 (12)	6.65 (13)	7.50 (7)	3.56 (9)	5.29 (10)	6.75 (14)	7.64 (7)
b_2		8.22 (4)	11.7 (6)	11.2 (2)	5.66 (36)	8.32 (35)	11.9 (7)	11.1 (2)
$n(2s)$	1	2.00	2.00	2.00	2.00	1.92 (21)	1.97 (13)	2.00
$\kappa(2s)$		1.01 (4)	0.95 (6)	0.96 (2)	1.06 (5)	1.05 (4)	0.98 (6)	0.99 (2)
$n(2p_x(=2p_y))$	2	0.41 (6)	0.39 (8)	0.47 (3)	0.21 (8)	0.16 (13)	0.13 (7)	0.07 (3)
$\kappa(2p_x(=2p_y))$		0.58 (7)	0.70 (11)	0.49 (1)	0.50 (8)	0.53 (10)	0.97 (39)	0.86 (21)
$n(2p_z)$	1	0.50 (19)	0.61 (21)	0.69 (9)	0.45 (17)	0.55 (39)	0.66 (28)	0.81 (12)
$\kappa(2p_z)$		0.97 (17)	0.97 (21)	0.87 (6)	0.99 (32)	0.96 (16)	0.98 (18)	0.88 (4)
c_{311}		**−10.6 (47)**	−5.46 (622)	**−4.65 (235)**	**4.9 (48)**	**−12.0 (52)**	−5.3 (64)	**−4.9 (23)**
c_{333}		−4.98 (1139)	−2.85 (1560)	**−4.93 (396)**	−8.0 (102)	−5.7 (133)	−2.7 (168)	**−5.7 (39)**
q_{1111}		0.56 (251)	−2.62 (285)	−0.41 (101)	0.5 (22)	−1.6 (29)	−0.7 (14)	**−1.7 (12)**
q_{3333}		**−23.0 (152)**	**−19.4 (129)**	**−8.08 (352)**	1.3 (71)	**−51.3 (189)**	1.9 (133)	**−8.5 (36)**
q_{1122}		−2.59 (732)	1.03 (827)	2.94 (375)	−3.9 (69)	**−26.7 (90)**	9.4 (165)	**12.8 (36)**
q_{1133}		1.32 (1802)	**25.2 (205)**	**27.0 (60)**	−3.5 (151)	**63.4 (230)**	−11.7 (197)	**20.3 (62)**
Extinction								
Y_{11}		43.5 (51)	22.5 (62)	29.2 (13)	45.7 (78)	42.4 (51)	20.5 (48)	23.6 (9)
Y_{22}		17.3 (45)	25.3 (52)	38.1 (12)	21.6 (30)	18.9 (42)	24.5 (44)	28.4 (7)
Y_{33}		25.5 (14)	43.2 (36)	68.1 (31)	21.1 (15)	23.6 (18)	35.5 (18)	47.9 (17)
Y_{12}		−1.40 (328)	−12.0 (53)	3.90 (74)	−5.0 (28)	−2.7 (31)	−8.9 (43)	2.4 (5)
Y_{13}		0.40 (163)	20.0 (30)	−5.59 (117)	1.4 (18)	0.7 (15)	16.1 (21)	−4.2 (7)
Y_{23}		0.32 (19)	1.75 (250)	−0.88 (102)	1.2 (11)	2.7 (17)	1.5 (20)	−0.3 (6)

(APD; Kishimoto *et al.*, 1998) at the Photon Factory in Tsukuba by suppressing the statistical counting errors of all reflections less than 0.1% (Tanaka *et al.*, 2010). The XAO analysis of the data revealed the 5*d* peaks clearly and the $5d_{5/2}\Gamma_8$ orbitals were almost half-filled by electrons. In the present study $5d_{5/2}\Gamma_8$ orbitals are fully occupied at 100 K and partially occupied at the other temperature, as listed in Table 3.

4.4. EDD around the B_6 moiety

The B—B bonds in SmB_6 are covalent ones. A molecular orbital (MO) model is necessary to analyze the EDD of the two-centre electrons around the centres of the B—B bonds. Since the two-centre bonding electrons in the centre of the B–B bonds cannot be taken into account in the XAO analysis, these peaks in Fig. 2 are not affected in Fig. 8 except at 100 K, where a negative EDD on the line of $(B—B)_{in}$ changed to a positive one. It must also be pointed out that the MO treatment of the present system including the metal orbitals is not possible with the present accuracy of measurement, since the sum of the contributions from the two-centre scattering factors to each structure factor is smaller than the error of the intensity measurement in most of the reflections (Tanaka, 1996).

Since the B atom mentioned in Tables 2 and 3 is on the *z* axis, the $2p_z$ orbital contributes mainly to the B—B bond between the two B_6 octahedra. The B—B bonds in the B_6

octahedron are composed mainly of $2p_x$ and $2p_y$ orbitals. The two types of bonds are called $(B-B)_{out}$ and $(B-B)_{in}$, respectively. Since the $2p_x$ and $2p_y$ electrons are transferred from the B_6 moiety to the $5d$ orbitals as $n(2p_x)$, $n(2p_y)$ and $n(5d_{5/2}\Gamma_8)$ in Table 3 show, the relation between the residual density around B_6 in Figs. 2 and 8, and the populations of the $2p$ orbitals becomes interesting. The populations on $2s$ are 2.0 within experimental error. Those of $2p_{x,y}$ and $2p_z$ decrease and increase, respectively, with an increase in temperature. The number of $2p$ electrons in B ranges from 0.86 to 0.95 and each B atom has a positive charge ranging from +0.05 to +0.14. Accordingly each Sm has a negative charge ranging from −0.84 to −0.30. This is the reason why the $5d_{5/2}\Gamma_8$ state lies lowest among the $5d$ states. The peaks of the covalent bonds on $B-B_{in}$ have a height of −0.09, 0.31, 0.22 and 0.11 e Å^{-3} at 100, 165, 230 and 298 K, respectively, in Fig. 2 after the spherical-atom refinement. The peak at 100 K becomes positive in Fig. 8 and the negative area of EDD decreases as a whole after refinement (III), since better AO models were introduced to explain the aspherical EDD by the XAO analysis and made the structure factors more precise.

4.5. Analysis of anharmonic vibration

The parameters for anharmonic vibration (AHV) in Tables 2 and 3 were also introduced in refinements (I)–(III). They were refined simultaneously with the other parameters. However, since X-rays are scattered by electrons and not by nuclei, the temperature factors obtained by X-ray diffraction correlate strongly with the aspherical EDD. The vibronic potentials of Sm and B are expressed in terms of the parameters q_{iijk} and c_{ijk} in equations (3) and (4). Each parameter specifies the direction of the vibration of the atom. For example, q_{1111} and q_{1122} express the anharmonic vibration along ⟨100⟩ and ⟨110⟩. Since the directions which harmonic and anharmonic parameters specify usually overlap, the parameters of harmonic and anharmonic vibration correlate strongly and they were refined alternately.

A negative AHV parameter indicates preferential AHV along the direction specified by it. q_{1111} of Sm in Table 3 is positive except at 230 K where q_{1111} is zero within experimental error, and the $4f$ peaks at 230 K, which are the highest peaks among the others shown in Fig. 1, reflect more preferential AHV along ⟨100⟩ than that at the other temperatures. Similar enhanced EDD by anharmonic vibration was also found in CeB_6 at 165 K (Tanaka & Ōnuki, 2002). The negative peaks along ⟨110⟩ around Sm at 298 K in Fig. 1(*d*) correspond to the inhibited AHV along ⟨110⟩ or to positive q_{1122} (which is negative at the other temperature). Since the aspherical features of the difference density in Fig. 1 are not modified by the spherical atomic orbitals but correspond directly to the observed aspherical EDD, the AHV parameters correspond well to the aspherical features of the difference density in Fig. 1. This indicates that the AHV parameters were refined well.

5. EDD and the properties of SmB_6

5.1. Metallic behaviour of SmB_6 and $5d$ electrons

The electrical resistivity of SmB_6 measured by Allen *et al.* (1979) increases gradually like semi-conductors below room

Figure 6
Difference densities around Sm after refinement (II). Note that (*a*), (*b*) and (*c*) are at 165, 230 and 298 K, respectively. Contours are as in Fig. 1.

temperature and begins to show a steep increase below 30 K with a decrease in temperature. It also begins to increase like metals above room temperature with an increase in temperature (Ueda & Ōnuki, 1998). The difference density after aspherical-atom refinement in Fig. 1 clearly reveals that at 298 K Sm is surrounded by a spherical and negative region, while at the other temperatures there is no such region. It seems to correspond to the rising of the resistivity and indicates that electrons are conducted through the overlapped Sm-5d and B-2$p_{x,y}$ orbitals illustrated in Fig. 4. The conduction band consists mainly of the 2p and 5d orbitals (Kimura *et al.*, 1990). This is the reason why $n(2p_{x,y})$ is much smaller than 0.5 and $n(5d_{5/2}\Gamma_8)$ has a significant value, as listed in Table 3. Since the direction of the $2p_z$ orbital is perpendicular to the direction from Sm to the centre of the B—B_{out} bond, it is expected that $2p_z$ does not overlap well with the 5d orbitals of Sm and thus it is localized mainly on the B—B_{out} bond.

The changes in $n(p_{x,y})$ and $n(5d_{5/2}\Gamma_8)$ with temperature shown in Table 3 are similar to that of the resistivity of SmB_6 although the errors are still too large. $n(5d_{5/2}\Gamma_8)$ increases smoothly with temperature from 230 to 100 K, and also increases at 298 K compared with that at 230 K. $n(2p_{x,y})$ of B after refinement (III) in Table 3 increases smoothly with decreasing temperature, whereas that of $2p_z$ of B decreases. It may then be proper to consider that the increase in populations of $2p_{x,y}$ and $5d_{5/2}\Gamma_8$ orbitals, which are comprised in the conduction band, corresponds to the increase in electrons localized at the orbital and thus makes the resistivity higher. However, the populations are not equal to the number of electrons localized or fixed to the atom, but are proportional to it, since $5d_{5/2}\Gamma_8$ orbitals at 100 K are fully occupied, although SmB_6 shows a smooth change in the resistivity with temperature below 100 K. These facts indicate that there is a relationship between the populations of orbitals which consist of the conduction band and the resistivity.

5.2. Unoccupied $4f_{7/2}\Gamma_6$ at 100 K and Kondo insulator

SmB_6 has an energy gap of 27 K (= 2.3 meV) between 4f states and the conduction band, which may depend on temperature (Ueda & Ōnuki, 1998). Dieke *et al.* (1968) calculated energies of the excited states of lanthanides with the spin-orbit interaction model. They show that the energy gaps between the ground state and the first excited states of Sm^{3+} ($4f_{7/2}$) and of Eu^{3+} ($4f_1$) are smaller than those of the other lanthanides. Therefore, the $4f_{7/2}\Gamma_6$ state, which is the most stable among the J = 7/2 states, is closer to the highest state $4f_{5/2}\Gamma_7$ in the ground state of Sm^{3+} in the O_h crystal field. These facts support the occupation of $4f_{7/2}\Gamma_6$ in the present study, except at 100 K.

The energy gap between $4f_{5/2}$ and $4f_{7/2}$ bands of SmB_6 was calculated to be 27 meV by LSDA + U (Antonov *et al.*, 2002) and to be less than 13 meV by the self-consistent linearized augmented plane wave (LAPW) method (Yanase & Harima, 1992). It was observed that the energy gap between 4f states exists at 100 K and it was lost between 100 and 150 K in several experiments such as the ESR (Al'tshuler *et al.*, 1986), specific heat measurement (Kasuya *et al.*, 1979) and photoemission spectroscopy (Souma *et al.*, 2002). SmB_6 shows a steep increase in the resistivity below 30 K and SmB_6 is known as a Kondo insulator. These facts support our results that $4f_{7/2}\Gamma_6$ is occupied except at 100 K, which seems to indicate that a band gap is formed between 4f states at 100 K.

5.3. Lattice parameter at 100 K and change in the B—B bond lengths with temperature

The lattice parameter changes significantly in Fig. 9 when

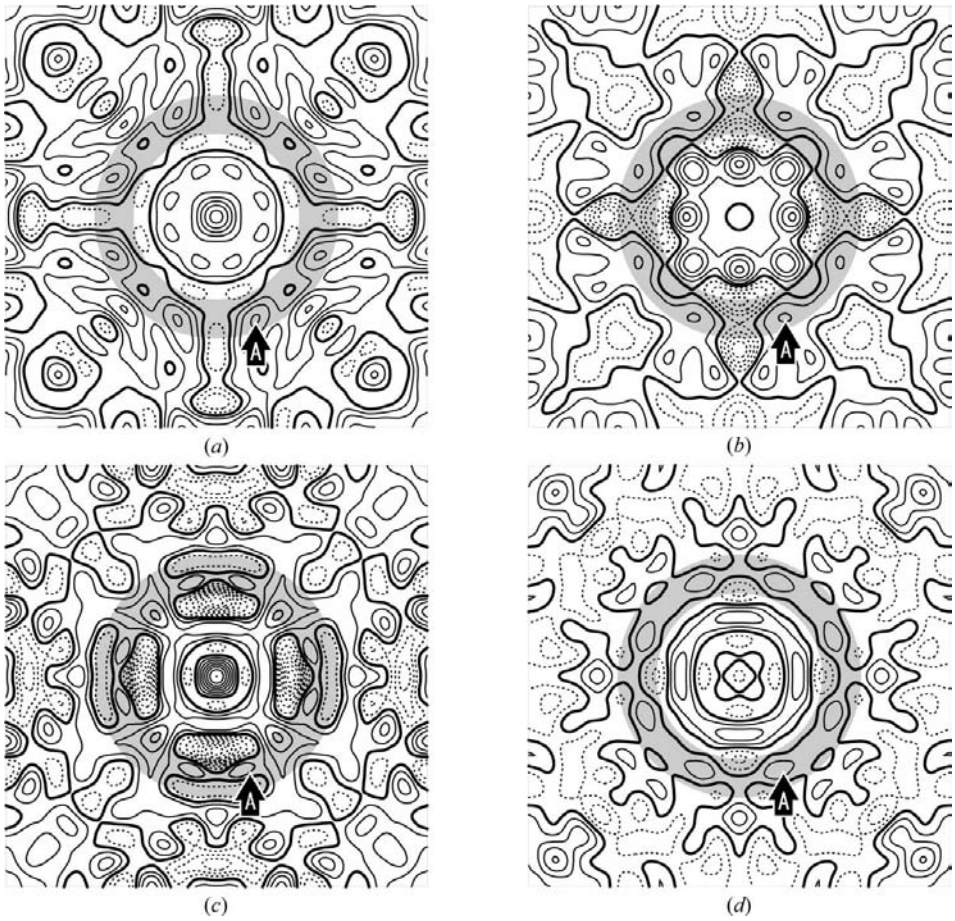

Figure 7
Difference densities around Sm after refinement (III). (*a*), (*b*), (*c*) and (*d*) are at 100, 165, 230 and 298 K, respectively. Contours are as in Fig. 1.

temperature decreases, although the change is very small because the crystal is very hard. The temperature factors of Sm and B were also reduced four or five times more than their errors with temperature. The lattice parameter of SmB_6 was reported to be minimum near 150 K by Menth, Buehler, Levinstein & Geballe (1969) and Mercurio *et al.* (1976). It was attributed to the change in ratio of Sm^{3+} and Sm^{2+} (Tarascon *et al.*, 1980). In the present study the lattice parameter was reduced from 298 to 165 K, but becomes longer at 100 K than that at 165 K by 0.0008 (3) Å, although the difference is within three times the error. In CeB_6 the lattice parameter was reduced smoothly from 298 to 100 K (Tanaka & Ōnuki, 2002). In the present study the outermost and bulky $5d_{5/2}\Gamma_8$ orbitals are fully occupied and $2p_{x,y}$ orbitals, which expand toward the ⟨100⟩ directions, are more populated at 100 K. Although the errors of the populations are large and the difference is not significant enough, $n(2p_x(=2p_y))$ evidently has a tendency to increase with a decrease in temperature (Table 3). $\kappa(2p_x(=2p_y))$ at 100 K in Table 3 shows that $2p_{x,y}$ orbitals expand. These results indicate that one of the reasons of the expansion of the lattice parameter of SmB_6 below 165 K is the increase in the occupation of the $5d_{5/2}\Gamma_8$ orbitals.

Parameter z of B is the only coordinate to be refined. It was reduced by 0.0008 (2), 0.0025 (3) when temperature decreased from 298 to 230 K, and 230 to 165 K, but increased by 0.0031 (4) from 165 to 100 K. The increase in z reduces the bond length of $(B-B)_{out}$. Since all the B atoms were located on the edges of the cubic unit cell, the lattice parameter a is expressed in terms of the B—B bond lengths as

$$a = 2^{1/2}(B-B)_{in} + (B-B)_{out}. \quad (5)$$

When the population of B-$2p_z$ increases, the $(B-B)_{out}$ bond becomes stronger and shorter, and makes z increase, and *vice versa* for $(B-B)_{in}$. The change in the B—B bond lengths with temperature is illustrated in Fig. 10. In our previous study (Tanaka & Ōnuki, 2002), at 298 K the B—B bond lengths were expected to be affected by the occupied $4f_{5/2}\Gamma_7$ orbital located along ⟨111⟩ directions to the center of the B_6 octahedron, which was expected to make the B-$p_{x,y}$ orbitals unstable and makes the $(B-B)_{in}$ bond longer. Bulky $5d_{5/2}\Gamma_8$ is also expected to affect the bond lengths. $4f_{7/2}\Gamma_6$ orbitals form a spherical EDD on average and may not affect the bonds. $n(2p_z)$ after refinement (III) has a tendency to reduce on lowering the temperature, but $(B-B)_{out}$ and $(B-B)_{in}$ becomes respectively shorter and longer at 230 and 100 K. In the present study, however, relationships between the population parameters and the B—B bond lengths are not found.

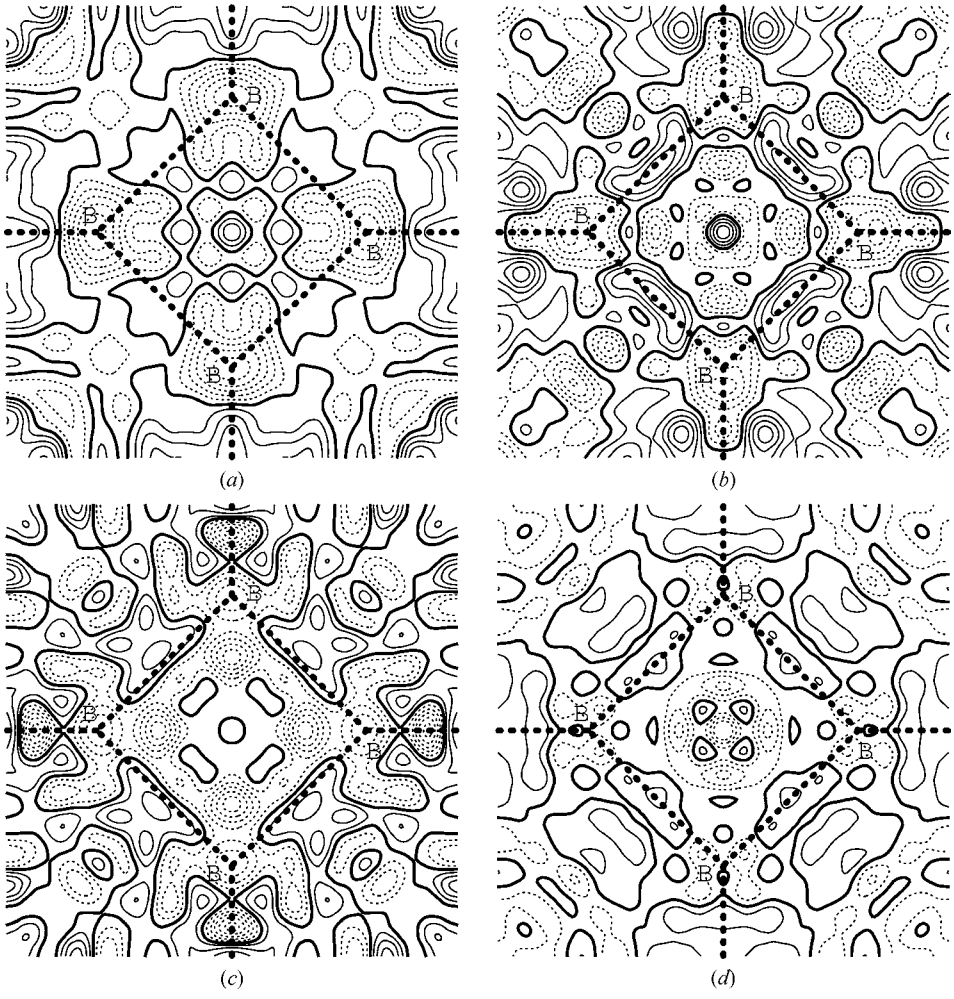

Figure 8
Difference densities around B on the plane $z = 0$ after refinement (I). (*a*), (*b*), (*c*) and (*d*) are at 100, 165, 230 and 298 K, respectively. Contours are as in Fig. 1.

5.4. Valence fluctuation in SmB_6

SmB_6 is known as a valence-fluctuating material and the valence of Sm fluctuates between $Sm^{3+}(4f^5)$ and $Sm^{2+}(4f^6)$. The ratio of Sm^{3+} and Sm^{2+} was reported to be between 7:3 ($Sm^{2.7+}$) and 6:4 ($Sm^{2.6+}$) (Menth, Buehler & Geballe, 1969; Cohen *et al.*, 1970; Tarascon *et al.*, 1980; Takigawa *et al.*, 1981). The numbers of 4*f* electrons after refinement (III) are 4.8 (6), 6.2 (5), 6.4 (5) and 5.2 (4), at 100, 165, 230 and 298 K, respectively. In refinement (III) 5*d* orbitals are occupied making the valence of Sm negative. If $n(5d_{5/2}\Gamma_8)$ is excluded from the calculation of the valence of Sm, it is 3.2 (6), 1.8 (5), 1.6 (5) and 2.8 (4) at 100, 165, 230 and 298 K. Although the errors are high, the

valence is closer to +3 at 100 and 298 K, and closer to +2 at 165 and 230 K within experimental error. However, the valence of Sm is not an integer number in the present study and cannot be compared with the investigations cited above.

6. Conclusion

The results are summarized below:

(i) When Figs. 1(*a*)–(*d*) after the spherical-atom refinement and the final residual density in Figs. 7(*a*)–(*d*) are compared, it is evident that 4*f*-EDD was successfully analyzed by XAO analysis based on the *j*–*j* coupling scheme.

(ii) $5d_{5/2}\Gamma_8$ orbitals are occupied at 100, 165, 230 and 298 K, which is supported by the improved difference-density maps at the 5*d* region.

(iii) Elongation of lattice parameters below 150 K in SmB_6, as reported earlier by Menth, Buehler, Levinstein & Geballe (1969), may be explained by the occupied $5d_{5/2}\Gamma_8$ orbitals at 100 K, although the accuracy of our measurement indicates that the elongation is stopped on lowering the temperature to 165 K.

(iv) $4f_{7/2}\Gamma_6$ orbitals are vacant at 100 K, although they are occupied at the other three temperatures. It may be correlated to the band gap between the 4*f* states, which is reported to start developing between 150 and 100 K (Souma *et al.*, 2002).

(v) $5d_{5/2}\Gamma_8$ orbitals correspond to the e_g orbitals in the strong field model. Among the 5*d* orbitals only the $5d_{5/2}\Gamma_8$ orbitals are occupied. This agrees with the results of the band calculation of LaB_6 by Harima (1988) that the $5d$-e_g orbitals consist of the conduction band with the 2*p* orbitals of the B atom. The occupation of 5*d* orbitals makes the Sm negative and B positive, which reverses the crystal field, and the energy level of the 5*d* orbitals originated from the $5d$-e_g orbitals becomes lower than the $5d$-t_{2g} orbitals. Therefore, the occupation of $5d_{5/2}\Gamma_8$ orbitals is also supported by the band theory.

(vi) The populations $n(5d_{5/2}\Gamma_8)$ and $n(2p_x)$, and the resistivity increase on lowering the temperature. The population increases at 298 K and the resisitivity begins to increase at around room temperature with rising temperatures showing the metallic character of SmB_6. These facts indicate a correlation between resistivity and the electron populations of the atomic orbitals which consist of the conduction band, since the population on the atomic orbital is proportional to the number of electrons localized on the atomic orbital.

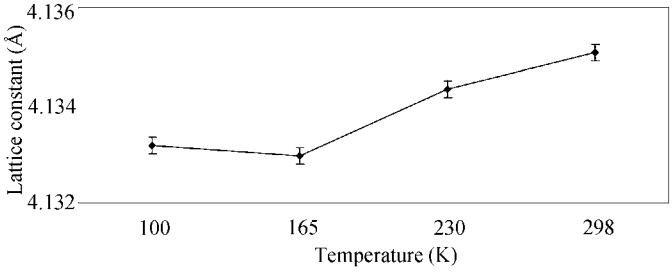

Figure 9
Temperature dependence of the lattice constant *a*.

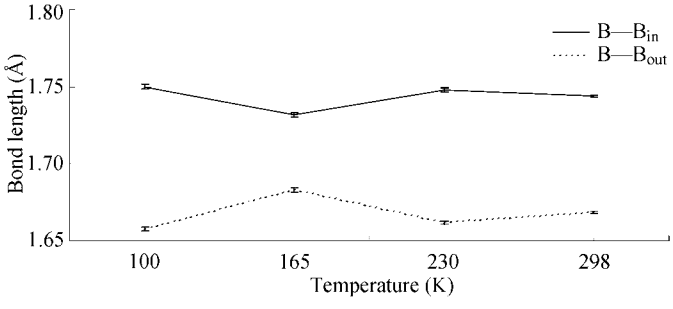

Figure 10
Temperature dependence of B—B bond lengths.

Authors wish to express their sincere their gratitude to Professor Isao Sakamot of the Physics Department of Nagoya Institute of Technology. They also wish to express their gratitude to JST (Japan Science and Technology Agency) for supplying a financial support in the program of Research for Promoting Technological Seeds.

References

Allen, J. W., Batlogg, B. & Wachter, P. (1979). *Phys. Rev. B*, **20**, 4807–4813.
Al'tshuler, T. S., Khaliullin, G. G. & Khomskii, D. I. (1986). *Sov. Phys. JETP*, **63**, 1234–1237.
Antonov, V. N., Harmon, B. N. & Yaresko, A. N. (2002). *Phys. Rev. B*, **66**, 165209-1-9.
Becker, P. J. & Coppens, P. (1974*a*). *Acta Cryst.* A**30**, 129–147.
Becker, P. J. & Coppens, P. (1974*b*). *Acta Cryst.* A**30**, 148–153.
Becker, P. J. & Coppens, P. (1975). *Acta Cryst.* A**31**, 417–425.
Bond, W. L. (1951). *Rev. Sci. Instrum.* **22**, 344–345.
Cohen, R. L., Eibschüetz, M., West, K. W. & Buller, E. (1970). *J. Appl. Phys.* **41**, 898–899.
Dieke, G. H. & Crosswhite, H. M. (1963). *Appl. Opt.* **2**, 675–686.
Harima, H. (1988). Doctor thesis, Tohoku University, Japan.
Kamimura, H., Sugano, S. & Tanabe, Y. (1969). *Ligand field Theory and its Application.* Tokyo: Syokabo.
Kasuya, T., Takegahara, K. & Fujita, T. (1979). *J. Phys.* **40**, C5-308–C5-313.
Kimura, S., Nanba, T., Kunii, S. & Kasuya, T. (1990). *J. Phys. Soc. Jpn*, **59**, 3388–3392.
Kishimoto, S., Ishizawa, N. & Vaalstra, T. P. (1988). *Rev. Sci. Instrum.* **69**, 384–391.
Liberman, D. A., Cromer, D. T. & Waber, J. T. (1971). *Comput. Phys. Commun.* **2**, 107–113.
Makita, R., Tanaka, K. & Ōnuki, Y. (2008). *Acta Cryst.* B**64**, 534–549.
Makita, R., Tanaka, K., Ōnuki, Y. & Tatewaki, H. (2007). *Acta Cryst.* B**63**, 683–692.
Mann, J. B. (1968). Report LA3691. Los Alamos National Laboratory, New Mexico, USA.
Menth, A., Buehler, E. & Geballe, T. H. (1969). *Phys. Rev. Lett.* **22**, 295–297.
Menth, A., Buehler, E., Levinstein, J. & Geballe, T. H. (1969). *J. Appl. Phys.* **40**, 1006.
Mercurio, J. P., Etourneau, J., Nasalain, R. & Hagenmuller, P. (1976). *J. Less Common Met.* **47**, 175–180.
Nickerson, J. C., White, R. M., Lee, K. N., Bachmann, R., Geballe, T. H. & Hull, G. W. (1971). *Phys. Rev. B*, **3**, 2030–2042.

Sakurai, T. & Kobayashi, K. (1979). *Rep. Inst. Phys. Chem. Res.* **55**, 69–77.
Souma, S., Kumigashira, H., Ito, T., Takahashi, T. & Kunii, S. (2002). *Physica B*, **312–313**, 329–330.
Stevens, K. W. H. (1952). *Proc. Phys. Soc. A*, **65**, 209–215.
Takigawa, M., Yasuoka, H., Kitaoka, Y., Tanaka, T., Nozaki, H. & Ishizawa, Y. (1981). *J. Phys. Soc. Jpn*, **50**, 2525–2532.
Tanaka, K. (1988). *Acta Cryst.* A**44**, 1002–1008.
Tanaka, K. (1996). *Mol. Cryst. Liq. Cryst.* **278**, 111–116.
Tanaka, K. (2008). *RDEDIT*. Personal communication.
Tanaka, K., Kato, Y. & Ōnuki, Y. (1997). *Acta Cryst.* B**53**, 143–152.
Tanaka, K., Kumazawa, S., Tsubokawa, M., Maruno, S. & Shirotani, I. (1994). *Acta Cryst.* A**50**, 246–252.
Tanaka, K., Makita, R., Funahashi, S., Komori, T. & Zaw Win (2008). *Acta Cryst.* A**64**, 437–449.
Tanaka, K. & Marumo, F. (1983). *Acta Cryst.* A**39**, 631–641.
Tanaka, K. & Ōnuki, Y. (2002). *Acta Cryst.* B**58**, 423–436.
Tanaka, K. & Saito, Y. (1975). *Acta Cryst.* A**31**, 841–845.
Tanaka, K., Takenaka, ?Y., Sakakura, T. & Kishimoto, S. (2010). In preparation.
Tarascon, J. M., Ishikawa, Y., Chevalier, B., Etourneau, J., Hagenmuller, P. & Kasaya, M. (1980). *J. Phys.* **41**, 1141–1145.
Thornley, F. R. & Nelmes, R. J. (1974). *Acta Cryst.* A**30**, 748–757.
Travaglini, G. & Wachter, P. (1984). *Phys. Rev. B*, **29**, 893–898.
Ueda, K. & Ōnuki, Y. (1998). *Physics of Heavy Electron Systems*. Tokyo: Shokabo.
Walter, U. (1986). *Z. Phys. B*, **62**, 299–309.
Yanase, A. & Harima, H. (1992). *Prog. Theor. Phys.* **108**, 19–25.